Intermetallics 94 (2018) 1–9

Contents lists available at ScienceDirect

Intermetallics

journal homepage: www.elsevier.com/locate/intermet

Structural disorder effects on the magnetic entropy change of $DyCo_2$ intermetallic: Mechanical milling and the weakening of the itinerant electron metamagnetism mechanism

V.G. de Paula[a], M. Gomes Silva[b], L.M. da Silva[b,*], A.O. dos Santos[b], R. Lang[c], L. Otubo[d], A.A. Coelho[a], L.P. Cardoso[a]

[a] Instituto de Física Gleb Wataghin, Universidade Estadual de Campinas - UNICAMP, 13083-859, Campinas, SP, Brazil
[b] Centro de Ciências Sociais, Saúde e Tecnologia (CCSST), Universidade Federal do Maranhão - UFMA, 65900-000, Imperatriz, MA, Brazil
[c] Instituto de Ciência e Tecnologia - ICT, UNIFESP, 12231-280, São José dos Campos, SP, Brazil
[d] Centro de Ciência e Tecnologia de Materiais, Instituto de Pesquisas Energéticas e Nucleares - IPEN/CNEN, 05508-000, São Paulo, SP, Brazil

ARTICLE INFO

Keywords:
A. Intermetallic compound
B. Mechanical milling
C. Nanocrystallites
D.Magnetic properties
E. Magnetic applications

ABSTRACT

Magnetocaloric properties of the intermetallic $DyCo_2$ compound (in the form of reduced size particles) and its correlations with the itinerant electron metamagnetism (IEM) phenomenon and structural disorders are investigated and discussed. Micrometric-sized particles were prepared by a mechanical milling technique for two low milling times (4 and 8 h) and characterized by means of X-ray diffraction, scanning and high-resolution transmission electron microscopy as well as magnetic measurements as a function of an applied external magnetic field and temperature. The results show that the particles have irregular-shaped and amorphous "edges/ledges" with embedded randomly oriented $DyCo_2$ nanocrystallites. The average particle size practically does not change with increasing milling time, whereas the average crystallite size is slightly diminished. In contrast, microstrain values that indicate lattice deformation degree were rather increased after the milling processes. Structural disorders and surface effects, features resulting from mechanical impact, disturb the Dy-Co sublattice coupling and weaken the IEM mechanism responsible for the high magnetocaloric effect found for the $DyCo_2$ bulk sample. For the milled samples, it was observed reductions in the peak intensity of the magnetic entropy change ($-\Delta S_M$) and substantial broadenings of the distribution profiles which have contributed to an increase of the working temperature range of the investigated magnetocaloric material.

1. Introduction

Since the discovery of the magnetocaloric effect (MCE) by Weiss in 1917 [1], both theoretical and experimental aspects of the MCE have been extensively studied. Particularly in the last decades, this subject has attracted great attention after the discovery of materials with giant MCE near room temperature [2–4]. From experimental point of view, new compounds synthesis have always been a fundamental step in searching for materials with improved magnetocaloric properties, and has provided remarkable results for different families of intermetallic compounds [5–9]. In this way, to explore and develop materials with high MCE at low magnetic field is one interesting research goal in the area. On the other hand, despite the importance of high peak values of isothermal magnetic entropy change ($-\Delta S_M$) and adiabatic temperature change (ΔT_{ad}); a narrow $-\Delta S_M$ peak profile is a limiting cooling efficiency factor, since a real magnetic refrigerator must be able to operate in a wide temperature range. Therefore, an important magnetocaloric parameter is the full width half-maximum (δT_{FWHM}) of the $-\Delta S_M$ peak, which estimates the operating temperature range of a magnetocaloric compound [10]. Enhanced δT_{FHWM} values are frequently observed in materials with multiple magnetic phase transitions, composites and multi-layered compounds [11–13]. Recently, magnetocaloric measurements of $GdAl_2$ milled samples have shown a broadened $-\Delta S_M$ peak profile that was assigned to a distribution of Curie temperature (T_C) values due to the structural disorders induced by a milling process [14]. Moreover, several experimental results point out the mechanical milling as a process capable of providing an improvement in different aspects of the magnetocaloric effect. Hu et al. observed in the milled $La_{0.7}Ce_{0.3}Fe_{11.6}Si_{1.4}C_{0.2}$ compound a dependence of hysteresis loss on particle size [15]. Pires et al. reported an increase of $\approx$23% in the $-\Delta S_M$ magnitude after short milling times for $Tb_5Si_2Ge_2$ sample that was attributed to the coupling between magnetic and

* Corresponding author.
E-mail address: luzeli.moreira@ufma.br (L.M. da Silva).

https://doi.org/10.1016/j.intermet.2017.12.009
Received 21 June 2017; Received in revised form 4 November 2017; Accepted 6 December 2017
Available online 04 January 2018
0966-9795/

structural transitions characteristic of the $R_5Si_2Ge_2$ family [16].

The RM_2 (R = rare earth, M = transition metal) family of alloys is one of the most studied concerning the MCE [17]. High angular magnetic moment J values associated with the R ions, the presence of first or second order magnetic phase transitions and low hysteresis are the main aspects related to the remarkable magnetocaloric properties observed for this family. In particular, cobalt-based alloys (RCo_2) are interesting since a magnetic instability of the Co sublattice leads to a metamagnetic first order transition for some compounds of this family [18,19]. The field dependent character of the metamagnetic transition is a consequence of the net magnetic moment induced in the Co 3*d* itinerant electrons by an applied magnetic field larger than some critical value. The exchange coupling between both magnetic sublattices (R sublattice and Co coupling) gives rise to the itinerant electron metamagnetism (IEM) phenomenon that is the origin for first order transitions with high $-\Delta S_M$ values exhibited by RCo_2 compounds [20]. Despite the magnetic and magnetocaloric properties of RM_2 compounds are well known for bulk material, few studies of these compounds in the form of particles with reduced size (micro or nanoparticles) were conducted. Therefore, a more complete understanding on the changes provided by reduction of particle size and its impact on the magnetic and magnetocaloric properties are still an ongoing interesting research subject.

In this work, we report on the material synthesis of $DyCo_2$ microparticles obtained by the mechanical milling technique in low milling times (4 and 8 h), as well a detailed structural, morphological, magnetic and magnetocaloric characterizations. In particular, high-resolution transmission electron microscopy was employed as a direct observation tool to provide a consistent picture of the correlation between structural and magnetic properties. Notably, the results show that the microparticles have irregular-shaped with some amorphous “edges/ledges” and are formed by embedded randomly oriented $DyCo_2$ (single phase) nanocrystallites. The average particle size remained practically constant with increasing milling time, whereas the average crystallite size is slightly diminished. On the other hand, microstrain values (when compared to the bulk sample) were considerably increased. Such a structural disorder induced by the mechanical milling is presented and discussed. In short, the occurrence of lattice deformation disturbs the Dy-Co sublattice coupling and as a result, weakens the IEM mechanism that diminishes the $-\Delta S_M$ peak intensity and extends remarkably the MCE temperature range.

2. Experimental details

A $DyCo_2$ ingot (≈6 g) was prepared by arc melting of high purity elements (Dy = 99.9% and Co = 99.95%, both acquired from Sigma-Aldrich S.A.) in an argon (Ar) atmosphere. Subsequently, the alloy was annealed at 800 °C for five days. The material was then crushed and milled in a planetary ball mill (Fritsch Pulverisette7) at a rotation speed of 200 rpm using a hardened steel container also under Ar atmosphere. The milling was carried out in a sequence of 30 min milling and 10 min resting. The every 2 h the container was opened to uncompressing the powder. Amounts of material were collected after 4 and 8 h of milling for the undertaking of studies.

Powder X-ray diffraction (XRD) measurements were performed at room temperature by using a Rigaku Miniflex II diffractometer with Cu-Kα_1 (1.5406 Å) radiation. The diffraction patterns were obtained in the 2θ range between 20° and 80° with steps of 0.02° and acquisition time of 2 s. Crystalline phase was identified through the Rietveld refinement using the GSAS program [21]. The morphology and structure of the powders were analyzed and characterized by scanning electron microscopy (SEM) observations (Philips XL30 Electron Microscope - operated at an accelerating voltage of 20 kV) and by high-resolution transmission electron microscopy (HRTEM) images (JEOL JEM-2100 operating at 200 kV). SEM samples were prepared by directly spreading the powders over a conducting carbon double-sided tape and coated with Au by sputtering. TEM samples were prepared by dropping isopropanol sample suspensions on 400 mesh copper grid coated with a collodion film.

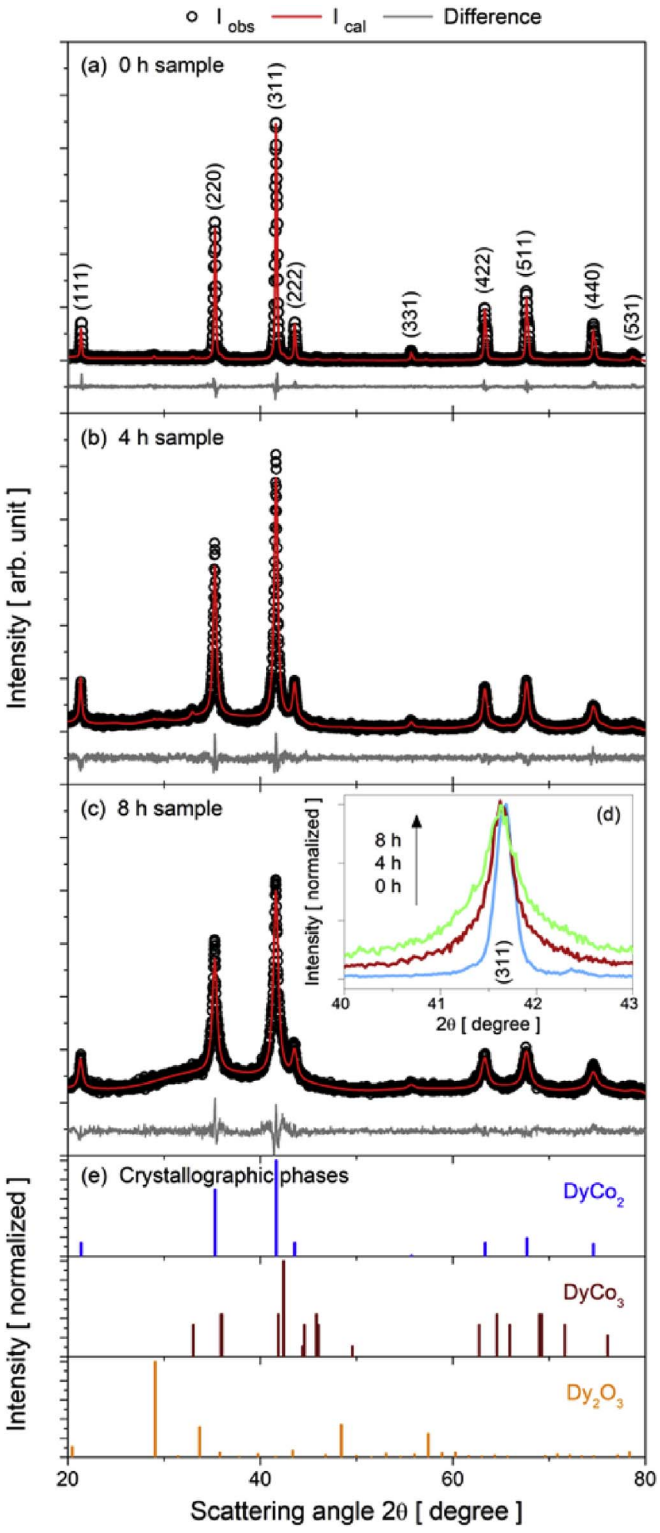

Fig. 1. X-ray diffraction and Rietveld refinement patterns of the $DyCo_2$ samples: (a) bulk (0 h) and milled (b) for 4 h and (c) for 8 h. All reflections belong to cubic $MgCu_2$ FCC structure. (d) Evolution in detail of the 311 reflection peak (normalized) with increasing milling time. (e) Crystallographic phases identified in the XRD patterns: $DyCo_2$, $DyCo_3$ and Dy_2O_3.

A superconducting quantum interference device magnetometer (MPMS SQUID magnetometer from Quantum Design Inc.) was

Table 1
From Rietveld refinement: lattice parameter, unit cell volume, average crystalline size, microstrain, R factors (R_{wp} and R_p) and goodness of fit (S) for each sample.

Milling time [hours]	Lattice parameter [Å]	Unit cell volume [$Å^3$]	Average crystallite size [nm]	Microstrain [%]	R_{wp} [%]	R_p [%]	S
0	7.194(1)	372.3(2)	156 ± 12	0.08	8	6	1.1
4	7.196(2)	372.6(3)	30 ± 3	0.53	11	9	1.2
8	7.197(2)	372.8(3)	24 ± 2	1.20	9	7	1.1

employed to measure the magnetization in the temperature range between 2 and 300 K under applied magnetic fields up to 50 kOe. The temperature dependences of magnetization M(T) were obtained following measurement protocols: zero-field-cooling (ZFC) and field-cooled-cooling (FCC). In the former, the samples were cooled down starting from room temperature under zero magnetic field. After stabilizing the temperature at 2 K the magnetic field was applied and then M(T) curves were recorded as a function of the increasing temperature (ZFC protocol). In the FCC protocol, the M(T) data were acquired while sweeping down the temperature from 300 to 2 K under an external magnetic field.

3. Results and discussion

Fig. 1(a) and (b) and 1(c) show the XRD patterns obtained for three $DyCo_2$ samples: the unmilled (referred to as bulk or 0 h) and the milled for 4 and 8 h, along with the calculated patterns using Rietveld refinement. Table 1 summarizes the lattice parameter, unit cell volume, average crystallite size, microstrain and the refinement reliability factors obtained for each sample. The analysis confirms that all the samples crystallize in the cubic $MgCu_2$ FCC structure and no evidence of contamination from the milling materials or oxidation was detected by X-ray diffraction. Nevertheless, a few peaks with very low intensity appear in the XRD patterns (bulk and milled samples) and correspond to small amounts of the $DyCo_3$ (≈4%) and Dy_2O_3 (≈1%) extra phases. The identified crystallographic phases in the studied system are exhibited in Fig. 1(e). The lattice parameter (a = 7.194 Å) and the unit cell volume (V = 372.3 $Å^3$) obtained for bulk sample are in agreement with the values found in the literature [22] and no significant change was observed for the milled samples as shown in Table 1. However, the diffraction peak intensity decreases along with the corresponding broadenings; highlighting the structural changes induced by the milling process. The inset (Fig. 1(d)) depicts in detail the peak associated with the 311 reflection for the bulk and milled for 4 and 8 h samples. The peak intensities were normalized for a better visualization. The observed considerable increase in peak width as milling time increases (inset) suggest a decrease in crystallite size. On the other hand, the decrease in peak intensities and the increase in the background contribution point to an amortization process. Therefore, the XRD results indicate that the mechanical impact produces both, a reduction of crystallite size and an amorphization degree in the $DyCo_2$ samples. From XRD Rietveld refinement analysis the average crystallite size has decreased with the mechanical milling: from 156 nm ± 12 nm (bulk sample) to 30 nm ± 3 nm and 24 nm ± 2 nm for the 4 and 8 h samples, respectively. In contrast, the microstrain - a measure that indicates the lattice deformation degree were greatly increased: from 0.08% (bulk sample) to 0.53% and 1.2% for the 4 and 8 h samples, respectively. These results reflect the occurrence of a large lattice deformation (structural disorder). It is well known that a decreased crystallite size and an increased microstrain are commonly microstructural changes caused by milling processes [23–25].

Fig. 2 depicts SEM images of the $DyCo_2$ powders after milling for (a) 4 and (b) 8 h. As can be noticed, the powders consist of irregular-shaped microstructures. Because of their irregular-shaped microstructures and agglomerates, the average particle size distributions were manually measured from the SEM images. In the measurements the Image-Pro Plus software (Media Cybernetics, Inc.) was used by considering the particles size as an approximation of diameter, and choosing the particles with loosely edges. Table 2 shows the quantitative results extracted from histograms analysis of the SEM images. The histograms were better fitted using the lognormal density function. The average particle size estimated for the sample milled for 4 h (Fig. 2(a)) is about 2.43 μm ± 1.18 μm, ranging from 0.79 to 9.46 μm, while for the sample milled for 8 h (Fig. 2(b)) is about 2.46 μm ± 0.91 μm, ranging from 0.48 to 5.79 μm. Although the lognormal fitting for the 4 h sample data have provided a slightly smaller value in average particle size than that of 8 h sample, their dispersion have shown to be slightly larger. In addition, the average sizes of the larger and smaller particles have decreased with increasing milling time. In summary, the histogram results demonstrate a very slight tendency of decreasing particle size with increasing milling time.

Bright-field TEM images of the samples milled for 4 and for 8 h in low magnification are show in Fig. 3(a) and (b), respectively. Micrometric-sized particles very dark (because of their size and thickness) can be observed. Even after the samples were dispersed in isopropanol, the particles were somewhat agglomerated, but the size and morphology of the particles could still be inferred. For statistical reasons, it was considered the size distribution from the SEM analysis, for which the population counted was about 300 particles. It is very hard to measure the same amount by means of TEM. Even though, was estimated a particle size distribution, reaching a mean size of 2.30 μm ± 0.90 μm (N = 11) and 1.91 μm ± 0.50 μm (N = 26) for the 4 and 8 h samples, respectively. The average size is a little smaller than the encountered by SEM because the measured population is very small for the TEM images as mentioned before.

Fig. 4 exhibits HRTEM images taken along the “edges/ledges” of particles shown in Fig. 3. The microscopies of the samples milled for 4 h (Fig. 4(a)) and for 8 h (Fig. 4(b)) reveal representative features of both samples. The high resolution of the technique makes it possible to detect several amorphous features produced by mechanical milling and in some cases to observe randomly oriented nanocrystalline grains. The amorphous thicknesses are not homogeneous along the edges/ledges of the particles. A larger single grain than those of same particle analyzed in Fig. 4(b) is shown in Fig. 4(c) and where a Fourier analysis was performed (Fig. 4(d)). The indexing of the fast Fourier transform (FFT) pattern obtained of the selected area matches with the $DyCo_2$ FCC structure (*Fd3m* space group). The respective zone axis (B) is depicted in Fig. 4(d). Therefore, the microparticles are constituted by embedded $DyCo_2$ nanocrystallites and by amorphous edges/ledges of inhomogeneous thickness.

Temperature dependence of magnetization following the ZFC and FCC protocols are exhibited in Fig. 5(a). For the sake of simplicity, only two representative sample curves are shown. The magnetization curves obtained from the sample milled for 4 h exhibited a similar behavior to that of the 8 h sample. $DyCo_2$ bulk sample presents ferromagnetic (FM) phase transition with Curie temperature (T_C) around 140 K. The magnetization derivative as a function of temperature, shown in Fig. 5(b), indicates that the milling process induces a very small broadening in the FM transition. No expressive alteration in the T_C value was observed even for the higher milling time. The coincidence between ZFC and FCC curves depicted in Fig. 5(c), as a zoom around T_C for bulk and 8 h samples, confirms the absence of thermal hysteresis for both samples.

Fig. 6 shows the field dependence of magnetization for the samples studied. The magnetic hysteresis at T = 2 K is significantly increased with milling process whereas, the saturation magnetization (M_S) is reduced as the milling time increases. The M_S decrease can be explained by a weakening of long-range magnetic interaction caused by the lattice deformation (structural disorder) and surface effects, i.e. the reduction in the particles size leads to an increase in the surface magnetic ions number without nearest neighbours for establishing a long-range

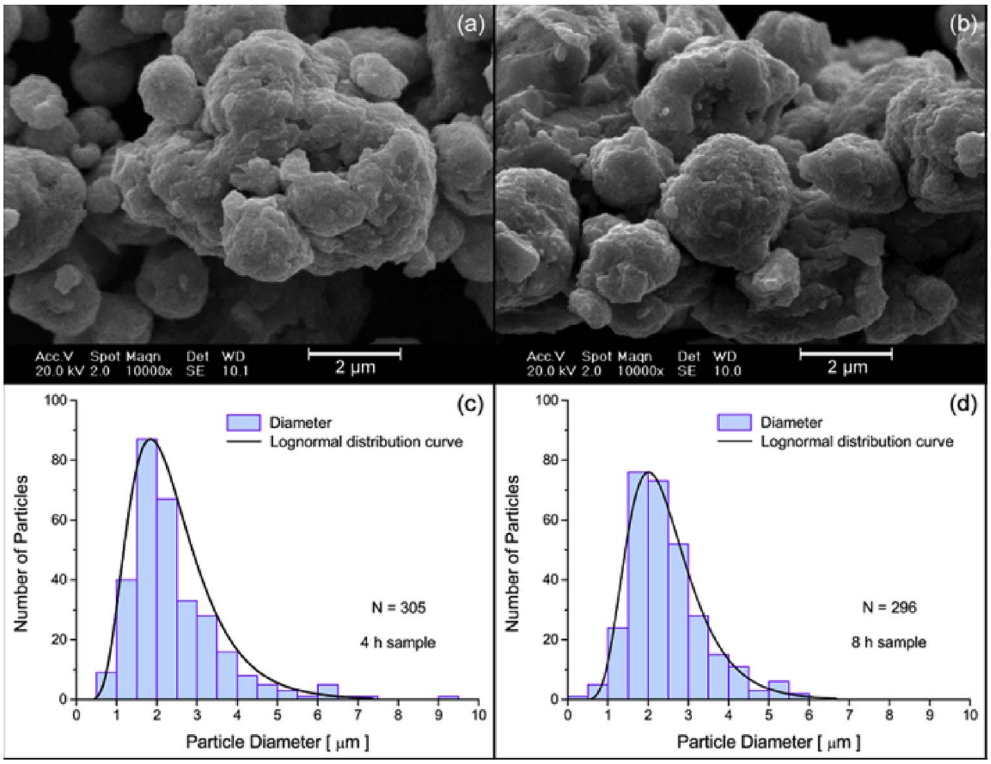

Fig. 2. SEM micrographs of the $DyCo_2$ powder milled for different times: (a) 4 h and (b) 8 h. The corresponding histograms are shown in (c) and (d), respectively.

Table 2
Values of average particle size, standard deviation and minimum and maximum size of the particles population obtained from histograms of the SEM images.

Milling time [hours]	Particles [number analyzed]	Average particle size [μm]	Standard deviation [μm]	Min./max. size [μm]
4	305	2.43	1.18	0.79/9.46
8	296	2.46	0.91	0.48/5.79

interaction. The remanent magnetization (M_R) increases from 1.68 μ_B/u.f. (bulk sample) to 3.32 μ_B/u.f. and 3.45 μ_B/u.f. (4 and 8 h samples, respectively) evidencing increments in the degree of spin alignment after removing the applied field in comparison to the bulk sample. The coercivity, the required field to remove M_R, gradually increases with the milling time increase: from 1.5 kOe (bulk sample) to 5.9 kOe (4 h sample) reaching 8.7 kOe for the 8 h sample.

Magnetic systems with small particles can present an enhanced anisotropy due to several factors such as: *i*) strong magnetic interaction (dipole-dipole and exchange interaction among neighbour particles) and *ii*) surface and shape of the particles, leading to an alteration of the anisotropy energy barriers [26–31]. The increasing in M_R values for the milled samples are possibly caused by different extra contributions of anisotropy. This anisotropy arises from the particles surface with fairly irregular shapes, surface disorders and interblock interaction effects in the ferromagnetic behavior that avoids the spins disorder to exhibit the same remanence observed for bulk sample. However, as temperature increases the M_R values are strongly decreased. For instance, the remanent magnetization for 8 h sample goes down to 0.74 μB/u.f. at T = 137 K (Fig. 6(b)) suggesting that thermal effects overcome anisotropic effects. The temperature dependence of M_R for the 8 h sample is shown in Fig. 6(c). Small remanent magnetization values around T_C are important for magnetic refrigeration applications once, hysteretic losses lower efficiency in the thermomagnetic cycles.

Magnetization isothermal curves M(H,T) as a function of applied magnetic field (0–50 kOe) measured around T_C (140 K) for the bulk and milled for 8 h samples are presented in Fig. 7(a) and (c), respectively. The magnetizations increase monotonically with the decrease of T as

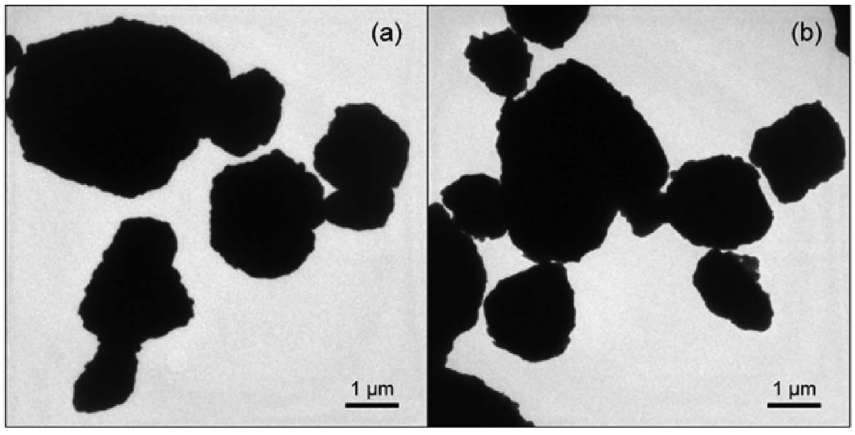

Fig. 3. Bright-field TEM images in low magnification of the $DyCo_2$ powders milled for different times: (a) 4 h and (b) 8 h.

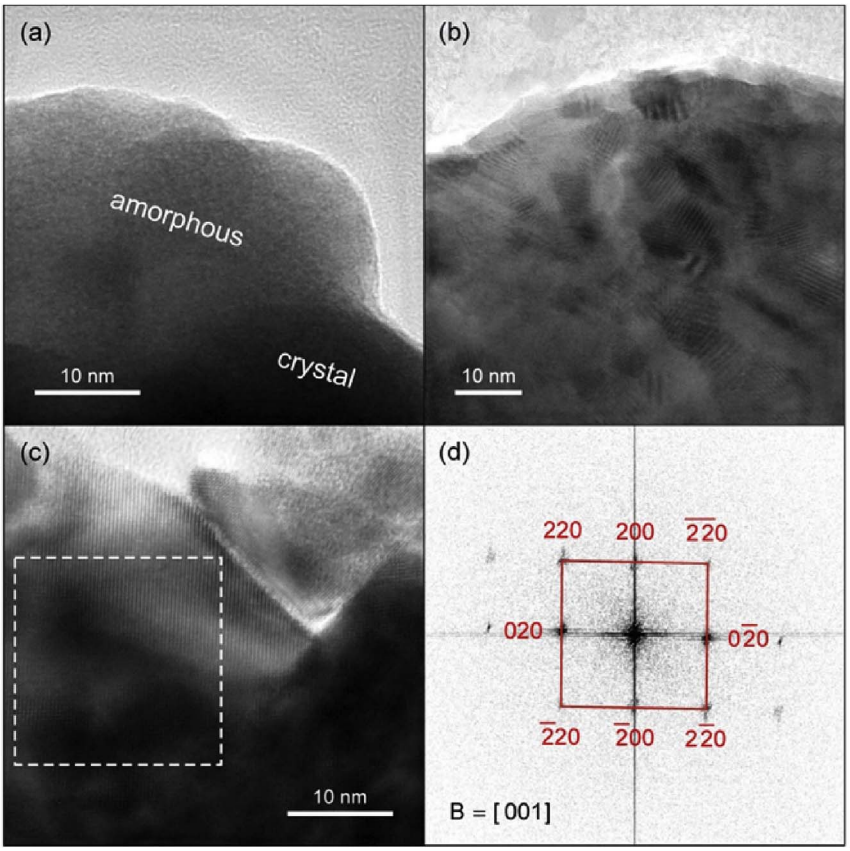

Fig. 4. HRTEM images of the $DyCo_2$ powders milled for different times: (a) 4 h and (b) 8 h (c) A single grain of the same particle in detail. (d) Fast Fourier transform (FFT) analysis of the selected area in (c). The FFT-pattern corresponds to the $DyCo_2$ FCC structure.

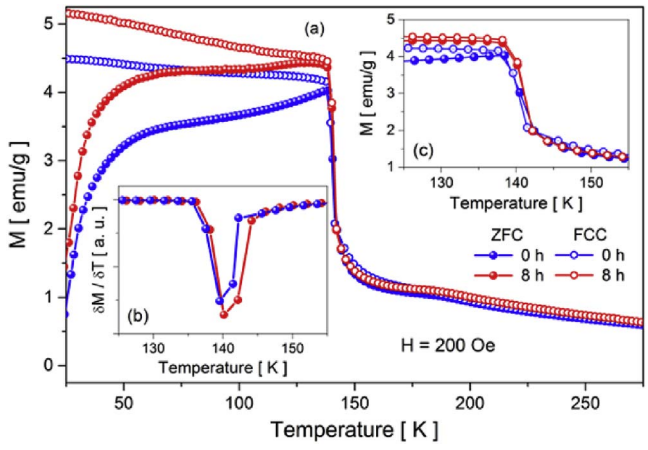

Fig. 5. (a) Temperature dependence of magnetization for $DyCo_2$ bulk and milled for 8 h samples following the zero-field-cooling (ZFC) and field-cooled-cooling (FCC) protocols. (b) Magnetization curve derivative for both samples. (c) ZFC and FCC curves in detail around T_C for a better visualization.

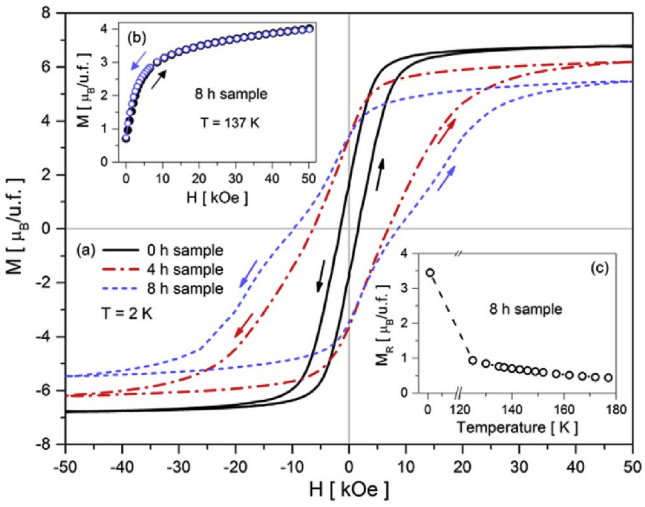

Fig. 6. (a) Magnetic hysteresis loops measured at 2 K for the $DyCo_2$ samples studied: bulk and the milled for 4 and 8 h. (b) Magnetization at 137 K as a function of magnetic field for the 8 h sample (increasing and decreasing) and (c) Remanent magnetization (M_R) as a function of temperature for the 8 h sample.

expected for a ferromagnetic material. The isothermal magnetization variation obtained for the 8 h sample is less pronounced in comparison to the bulk sample ones. In addition, the correspondent Arrot plots shown in Fig. 7(b) and (d) suggest changes in the nature of the FM transition. According to Banerjee criterion [16], a negative (positive) slope of Arrot plots is evidence of first-order (second-order) magnetic phase transition. Therefore, the negative slope on Arrot plot observed for bulk sample indicates first-order ferromagnetic transition, in agreement with the literature [5,10]. On the other hand, the 8 h sample shows a positive slope consistent with a second-order transition, which demonstrates that the milling process weakens the IEM mechanism responsible for the first-order ferromagnetic transition on $DyCo_2$.

The magnetocaloric effect, in terms of a magnetic entropy change ($-\Delta S_M$) was calculated from the isothermal magnetization curves by numerical integration of the Maxwell's relation [32]:

$$\Delta S_M(T, \Delta H) = \int_{H_i}^{H_f} \left(\partial M / \partial T\right)_H dH. \quad (1)$$

The temperature dependence of $-\Delta S_M$ for all $DyCo_2$ samples (bulk and milled for 4 and 8 h) calculated for different magnetic field changes (ΔH) varying up to 50 kOe is shown in Fig. 8. The magnetic entropy change curves for the bulk sample (Fig. 8(a)) display a positive peak

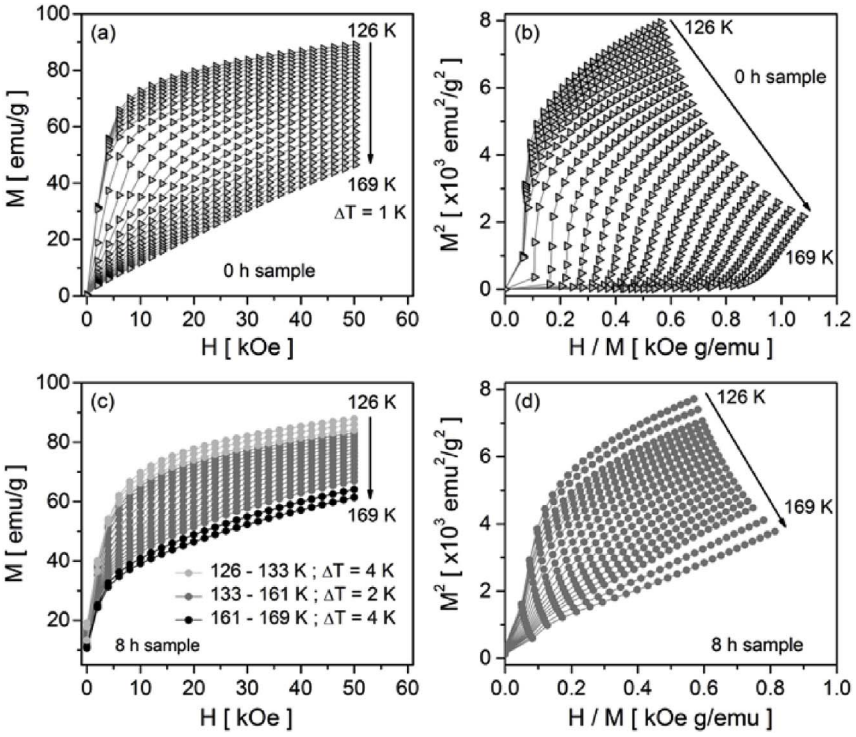

Fig. 7. Isothermal magnetization curves M(H,T) as a function of applied magnetic field (0–50 kOe) measured around T_C (140 K) for the $DyCo_2$ samples: (a) bulk and (c) milled for 8 h. The corresponding Arrot plots are shown in (b) and (d), respectively.

centered on T_C and that asymmetrically and substantially broadens to higher temperatures than 142 K as magnetic field change increases. For the milled samples, the $-\Delta S_M$ peak extends more symmetrically and its maximum shifts to higher temperatures with the increase of the external applied field. Furthermore, the shift and peak broadening are more pronounced for the 8 h sample as indicated by the hachured region in Fig. 8(c). Significant decreases in the peak intensities with the increase of the milling time are also observed.

Fig. 9(a) exhibits in particular a comparison between the $-\Delta S_M$ curves as a function of temperature for $\Delta H = 50$ kOe. The maximum value (peak) of magnetic entropy change ($\Delta S_M{}^{max}$) for the bulk sample is about 14.2 J/kgK. This value decreases to the milled samples: 8.2 J/kgK (4 h) and 5.1 J/kgK (8 h). Indeed, the $-\Delta S_M$ peak value decreases with decreasing crystallite size. Moreover, a peak profile broadening (δT_{FHWM}) as the milling time increases is clearly observed in the curves. Similar feature is also remarked for lower ΔH curves (see Fig. 8). Both

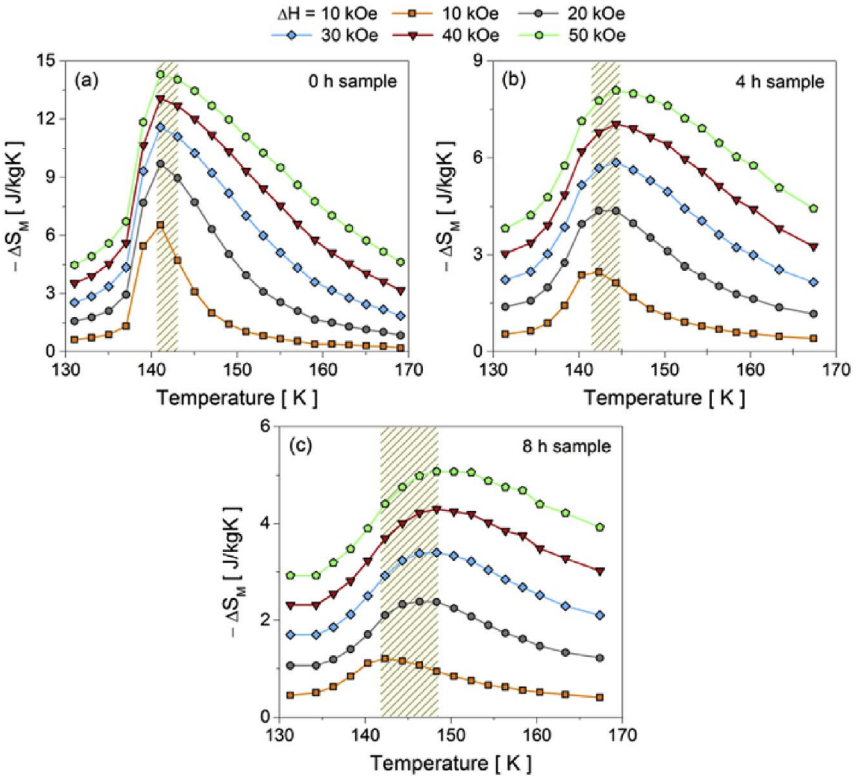

Fig. 8. Magnetic entropy change ($-\Delta S_M$) as a function of the temperature for different magnetic field changes for the $DyCo_2$ samples: (a) bulk and milled (b) for 4 h and (c) for 8 h.

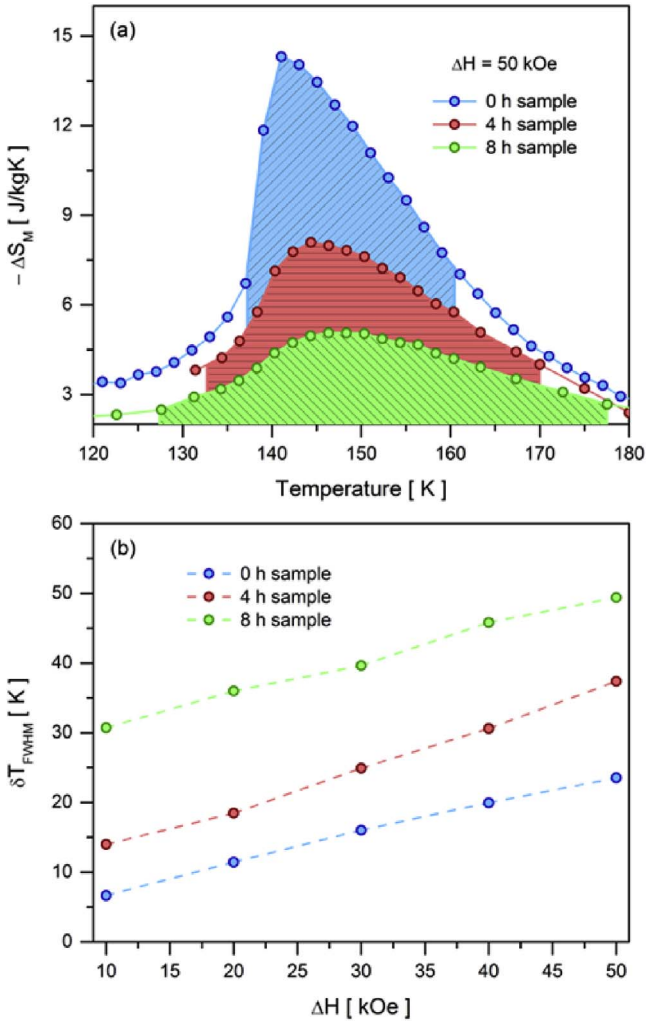

Fig. 9. Milling time effects on the magnetic entropy change ($-\Delta S_M$) curves for the $DyCo_2$ samples: bulk and milled for 4 and 8 h. (a) Magnetic entropy change as a function of temperature for ΔH = 50 kOe. The Hatching regions correspond to the area below the $-\Delta S_M$ curve in the full width at half-maximum (δT_{FHWM}). (b) δT_{FWHM} parameter as a function of magnetic field changes (ΔH) obtained from Fig. 8 data.

ΔS_M^{max} decrease and distribution-width increase suggest a second-order FM transition for the milled samples, consistent with Arrot plots results.

Let us explore the soundness of the statement that the first order metamagnetic transition of the bulk sample originates from the instability of the magnetic states associated with the Co sublattice. When the compound is cooled through the T_C, the molecular field (λ_M) coming from Dy ions induces the appearance of magnetic moments in Co ions, establishing a magnetic sublattice of 3*d* itinerant electrons. The presence of a critical external magnetic field (of the order of 4 kOe) induces an exchange coupling between both Dy-Dy and Co-Co magnetic sublattices characterized by a first order metamagnetic phase transition (IEM mechanism) in the $DyCo_2$ bulk sample. Several studies suggest that molecular field, ordering temperature, spin fluctuations and magneto-volume effects produced by chemical or mechanical pressure are critical parameters that govern the IEM mechanism in the mentioned compound [33–36]. For the milled samples, our case, the structural disorders (lattice deformation, atomic defects, amorphized regions, etc.) and surface effects (increase in the surface atoms number that do not participate on the long range interaction) straightly affect the long range RKKY interaction [37–39] and the molecular field. Hence, the change in the molecular field disturbs the coupling between Dy and Co magnetic sublattices and weakens the IEM mechanism. But how do the structural disorder and increased surface affect RKKY interaction? The

Table 3
ΔS_M^{max}, δT_{FHWM} and RCP values evaluated for two different magnetic fields change (ΔH): 10 and 50 kOe.

ΔH [kOe]	10			50		
Sample	Bulk	4 h	8 h	Bulk	4 h	8 h
ΔS_M^{max} [J/kgK]	6.5	2.4	1.1	14.2	8.2	5.1
δT_{FHWM} [K]	6.7	14.3	30.7	23.5	37.4	49.4
RCP [J/kg]	42.9	34.3	33.7	333.7	300.1	251.9

structural disorder causes different crystallites to be ordered at temperatures slightly different from each other. Thus, the macroscopic T_C ceases to be a delta function (nor is it in the bulk sample, since it is not defects free, i.e. the magnetic lattice is not continuous throughout the sample) and becomes the result of a T_C distribution and λ_M distribution. Surface atoms, however, decrease the amount of interacting magnetic ions causing a reduction in the RKKY strength. Therefore, the decrease of $-\Delta S_M$ observed for milled samples when compared with the bulk is understood as a result of both the weakening of long-range magnetic interaction caused by surface effects as well by the weakening the IEM mechanism caused by structural disorders.

The full width half-maximum (δT_{FHWM}) as a function of ΔH for each analyzed sample is presented in Fig. 9(b). There are quasi-linear dependencies, but the broadening magnitudes are rather different. For instance, the δT_{FHWM} broads about 113 and 358% when ΔH = 10 kOe and about 59 and 110% when ΔH = 50 kOe for the 4 and 8 h samples, respectively in comparison with the bulk δT_{FHWM} values (see Table 3). Nevertheless, reasonable decreases were estimated in the relative cooling power (RCP) for the same samples at 10 and 50 kOe. The RCP is considered as an important parameter to quantify the heat transferred between the hot and cold sinks in an ideal refrigeration cycle. The RCP was obtained by using the following approach [40]:

$$RCP = |\Delta S_M^{max}| \, \delta T_{FWHM}. \quad (2)$$

One notes that although there may be a decrease in the ΔS_M^{max} peak value, a large broadening of the distribution can cause an increase in the RCP value. A RCP around 43 J/kg was obtained for the bulk sample at ΔH = 10 kOe. The bulk value has decreased to approximately 34 J/kg for both the milled samples. At ΔH = 50 kOe, about 334 J/kg was obtained for the bulk and ≈300 and 252 J/kg for the 4 and 8 h samples, respectively. The largest broadening of the distributions and the smallest decreases in RCP values (both in terms of percentage) occur at lower magnetic fields change (ΔH = 10 kOe). Such result seems very interesting, since in principle the relationship of peak intensity *versus* broadening of the $-\Delta S_M$ distribution can be appropriately controlled by the milling process time.

In an ideal Ericsson cycle the magnetic material must operate in an optimal temperature range around ordering temperature, since its maximum efficiency is reached when the magnetocaloric effect exhibits constant temperature dependence. Such condition is not achieved using first-order bulk magnetic materials that present high values of magnetic entropy change; because most of these compounds exhibit a relatively narrow $-\Delta S_M$ peak. In this way, a controlled milling process can provide a better ΔS_M^{max} *versus* δT_{FHWM} correlation, improving the refrigerant material efficiency. In the present case, alterations in the ferromagnetic ordering induced by structural disorders and surface effects play a primary role in the δT_{FHWM}. On the other hand, the weakening of both IEM mechanism and the long range interaction are determining factors to reduce the intensity of ΔS_M^{max}.

By comparing the $DyCo_2$ results obtained here to other reported for mechanically milled intermetallic compounds, all suggest that the milling technique can be used as a versatile tool to synthesize new materials or to reduce dimensionality by providing improvements in magnetocaloric properties (decrease hysteresis, increase in $-\Delta S_M$ peak intensity, increase in δT_{FWHM} and RCP, etc.). High values of $-\Delta S_M$ were demonstrated for the $Pr_{1-x}Dy_xFe_9$ [41] and $Dy_xLa_{1-x}Ni_5$ [42] compounds

synthetized by mechanical milling. A table-like magnetocaloric effect between 30 and 165 K along with an enhanced magnetic entropy change below 30 K (related to a superparamagnetic behavior) were observed in $GdAl_2$ samples (microparticles with average size ≈ 1.3 μm) after 9 and 13 h of milling [14]. In $Tb_5Si_2Ge_2$ milled for 150 min (particles size ≈ 3.5 μm) an increase of ≈23% in the $-\Delta S_M$ peak intensity was achieved due to coupling between magnetic and structural transitions arising from internal strains promoted by the milling process [16]. A hysteresis loss reduction of ~61% was observed when $La_{0.7}Ce_{0.3}Fe_{11.6}Si_{1.4}C_{0.2}$ sample is ground from bulk to small particles (20–50 μm). Such a decrease was attributed to the increased surface area and decrease of internal strain and grain boundaries of the sample [15]. Decreases were also obtained in both thermal and magnetic hysteresis for $MnAs_{0.97}P_{0.03}$ alloys [43]. The results were discussed in terms of microstrain and partial amorphization induced by milling process. $Gd_5Si_{1.8}Ge_{1.8}Sn_{0.4}$ alloy submitted to a milling process also presented a decrease substantial in the thermal hysteresis as well as a RCP increase of ~35% (495 J/kg) when compared with the as-cast alloy (366 J/kg) [44]. Moreover, mechanical milling has also been used to produce $DyCu_2$ flakes [45] and decrease particle size of $ErCo_2$ [46]. Both compounds exhibited considerable broadening of the $-\Delta S_M$ peak and decrease in intensity. For the Pr_2Fe_{17} compound, broadening of ≈60% in δT_{FWHM} and increase in RCP were observed (430 J/kg for bulk sample and 573 J/kg for sample milled for 10 h) [47].

4. Conclusion

Mechanically milled $DyCo_2$ samples were studied by means of X-ray diffraction (XRD), scanning (SEM) and high-resolution transmission electron microscopy (HRTEM) as well magnetic measurements as a function of applied external magnetic field and temperature. SEM analyses combined with HRTEM observations revealed irregular-shaped microparticles with amorphous edges and/or ledges of inhomogeneous thickness, whose are constituted by embedded $DyCo_2$ nanocrystallites. The average particle size practically does not changed with increasing from 4 to 8 h the milling time, while the average crystallite size was slightly reduced. In contrast, there was a remarkable increase in lattice deformation degree pointed out by microstrain measurements. Increments in coercivity and remanence at low temperatures are ascribed to extra anisotropies contribution. The decrease of saturation magnetization is strongly correlated with structural disorders and surface effects, which among other factors weaken the long-range magnetic ordering and essentially disturb the *R*-Co sublattice coupling. As a result, the IEM mechanism responsible for high MCE values in $DyCo_2$ bulk is diminished for the milled samples. On the other hand, the $-\Delta S_M$ peak broadening induced by the milling process contributes to an increase of the working temperature range of $DyCo_2$ compound.

Summing up, the mechanical milling process can provide interesting changes in the intrinsic magnetic properties of bulk materials. In particular, the findings presented here can be an encouragement for further studies on the controlled milling effect in other first order magnetic systems, aiming a deeper understanding of the role played by the mechanical impact on the magnetocaloric properties and the improved efficiency of the refrigerant material.

Acknowledgements

The authors would like to thank the Brazilian founding agencies CNPq, FAPEMA and FINEP for partial financial support.

References

[1] A. Smith, Who discovered the magnetocaloric effect, Eur. Phys. J. 38 (2013) 507–517, http://dx.doi.org/10.1140/epjh/e2013-40001-9.
[2] J.R. Gómez, R.F. Garcia, A.D.M. Catoira, M.R. Gómez, Magnetocaloric effect: a review of the thermodynamic cycles in magnetic refrigeration, Renew. Suitable Energy Rev. 17 (2013) 74–82, http://dx.doi.org/10.1016/j.rser.2012.09.027.
[3] V.K. Pecharsky, K.A. Gschneidner Jr., A.O. Pecharsky, A.M. Tishin, Thermodynamics of the magnetocaloric effect, Phys. Rev. B 64 (2001) 144406, , http://dx.doi.org/10.1103/PhysRevB.64.144406.
[4] V.K. Pecharsky, K.A. Gschneidner Jr., Giant magnetocaloric effect in $Gd_5(Si_2Ge_2)$, Phys. Rev. Lett. 78 (1997) 4494, http://dx.doi.org/10.1103/PhysRevLett.78.4494.
[5] V.K. Pecharsky, K.A. Gschneidner Jr., Tunable magnetic regenerator alloys with a giant magnetocaloric effect for magnetic refrigeration from ~ 20 to ~ 290 K, App. Phys. Lett. 70 (1997) 3299–3301, http://dx.doi.org/10.1063/1.119206.
[6] A. de Campos, D.L. Rocco, A.M.G. Carvalho, L. Caron, A.A. Coelho, S. Gama, L.M. da Silva, F.C. Gandra, A.O. Dos Santos, L.P. Cardoso, Ambient pressure colossal magnetocaloric effect tuned by composition in $Mn_{1-x}Fe_xAs$, Nat. Mat. 5 (2006) 802–804, http://dx.doi.org/10.1038/nmat1732.
[7] A. de Campos, M. da Luz, A. de Campos, A. Coelho, L.P. Cardoso, A. dos Santos, S. Gama, Investigations in $MnAs_{1-x}Sb_x$: experimental validation of a new magnetocaloric composite, J. Magn. Magn. Mater. 374 (2015) 342–344, http://dx.doi.org/10.1016/j.jmmm.2014.08.069.
[8] R.D. dos Reis, L.M. da Silva, A.O. dos Santos, A.N. Medina, L.P. Cardoso, F.G. Gandra, Anisotropic magnetocaloric effect in $ErGa_2$ and $HoGa_2$ single-crystals, J. Alloys Compd. 582 (2014) 461–465, http://dx.doi.org/10.1016/j.jallcom.2013.08.023.
[9] R.D. dos Reis, L.M. da Silva, A.O. dos Santos, A.M.N. Medina, L.P. Cardoso, F.G. Gandra, Study of the magnetocaloric properties of the antiferromagnetic compounds RGa_2 (R= Ce, Pr, Nd, Dy, Ho and Er), J. Phys. Condens. Matter 22 (2010) 486002, , http://dx.doi.org/10.1088/0953-8984/22/48/486002.
[10] W.S. Zhang, E. Brück, Z.D. Zhang, O. Tegus, W.F. Li, P.Z. Si, D.Y. Geng, J.C.P. Klaasse, K.H.J. Buschow, Synthesis, structure and magnetic properties of $DyAl_2$ nanoparticles, J. Alloys Compd. 413 (2006) 29–34, http://dx.doi.org/10.1016/j.jallcom.2005.07.004.
[11] S.K. Giri, P. Dasgupta, A. Poddar, T.K. Nath, Large magnetocaloric effect and critical behavior in $Sm_{0.09}Ca_{0.91}MnO_3$ electron-doped nanomanganite, Eur. Phys. Lett. 105 (2014) 47007, http://dx.doi.org/10.1209/0295-5075/105/47007.
[12] P.J. Ibarra-Gaytán, J.L. Sánchez Llamazares, P. Álvarez-Alonso, C.F. Sánchez-Valdés, P. Gorria, J.A. Blanco, Magnetic entropy table-like shape in RNi_2 composites for cryogenic refrigeration, J. App. Phys. 117 (2015) 17C116, http://dx.doi.org/10.1063/1.4915480.
[13] R. Cabellero-Flores, V. Franco, A. Conde, K.E. Knipling, M.A. Willard, Optimization of the refrigerant capacity in multiphase magnetocaloric materials, App. Phys. Lett. 98 (2011) 102505, , http://dx.doi.org/10.1063/1.3560445.
[14] V.G. de Paula, L.M. da Silva, A.O. dos Santos, R. Lang, L. Otubo, A.A. Coelho, L.P. Cardoso, Magnetocaloric effect and evidence of superparamagnetism in $GdAl_2$ nanocrystallites: a magnetic-structural correlation, Phys. Rev. B 93 (2016) 094427, , http://dx.doi.org/10.1103/PhysRevB.93.094427.
[15] F.X. Hua, L. Chen, J. Wang, L.F. Bao, J.R. Sun, B.G. Shen, Particle size dependent hysteresis loss in $La_{0.7}Ce_{0.3}Fe_{11.6}Si_{1.4}C_{0.2}$ first order systems, App. Phys. Lett. 100 (2012) 072403, , http://dx.doi.org/10.1063/1.3684244.
[16] A.L. Pires, J.H. Belo, J. Turcaud, G.N.P. Oliveira, J.P. Araújo, A. Berenov, L.F. Cohen, A.M.L. Lopes, A.M. Pereira, Influence of short time milling in $R_5(Si, Ge)_4$, R = Gd and Tb, magnetocaloric materials, Mater. Des. 85 (2015) 32–38, http://dx.doi.org/10.1016/j.matdes.2015.06.099.
[17] A.M. Tishin, Y.I. Spichkin, The Magnetocaloric Effect and its Applications, first ed., CRC Press, Boca Ratón - USA, 2003 ISBN 0750309229.
[18] N.K. Singh, K.G. Suresh, A.K. Nigam, S.K. Malik, A.A. Coelho, S. Gama, Itinerant electron metamagnetism and magnetocaloric effect in RCo_2-based Laves phase compounds, J. Magn. Magn. Mater. 317 (2007) 68–79, http://dx.doi.org/10.1016/j.jmmm.2007.04.009.
[19] J. Herrero-Albillos, F. Bartolomé, L.M. García, F. Casanova, A. Labarta, X. Batlle, Nature and entropy content of the ordering transitions in RCo_2, Phys. Rev. B 73 (2006) 134410, , http://dx.doi.org/10.1103/PhysRevB.73.134410.
[20] R.Z. Levitin, A.S. Markosyan, Itinerant metamagnetism, Sov. Phys. Usp. 31 (1988) 730–749, http://dx.doi.org/10.1070/PU1988v031n08ABEH004922.
[21] A. Larson, R. Von Dreele, General Structure Analysis System (GSAS), Report: LAUR Los Alamos National Laboratory, Los Alamos, NM, 2004, pp. 86–748.
[22] A.S. Markosyan, Distortion of crystal structure and magnetostriction in the compounds RCo_2 (R = yttrium, dysprosium, holmium, erbium), Sov. Phys. Solid State 23 (1981) 965.
[23] D.P. Rojas, L.F. Barquín, J.S. Marcos, C. Echevarria-Bonet, J.I. Espeso, J.R. Fernández, L.R. Fernández, M.H. Mathon, Magnetic disorder in $TbAl_2$ nanoparticles, Mat. Res. Exp. 2 (2015) 075001, , http://dx.doi.org/10.1088/2053-1591/2/7/075001.
[24] C. Echevarria-Bonet, D.P. Rojas, J.I. Espeso, J.R. Fernández, M. de la Fuente Rodríguez, L.F. Barquín, L.R. Fernández, P. Gorria, J.A. Blanco, M.L. Fdez-Gubieda, E. Bauer, F. Damay, Magnetic phase diagram of superantiferromagnetic $TbCu_2$ nanoparticles, J. Phys. Condens. Matter 27 (2015) 496002, , http://dx.doi.org/10.1088/0953-8984/27/49/496002.
[25] B. Maji, K.G. Suresh, X. Chen, R.V. Ramanujan, Magnetic and magnetocaloric properties of ball milled Nd_5Ge_3, J. Appl. Phys. 111 (2012) 073905, , http://dx.doi.org/10.1063/1.3700243.
[26] S. Azzaza, S. Alleg, J.-J. Suñol, Microstructure characterization and thermal stability of the ball milled iron powders, J. Therm. Anal. Calorim. 119 (2015) 1037–1046, http://dx.doi.org/10.1007/s10973-014-4281-6.
[27] K. Modi, S.M. Dolia, P.U. Sharma, Effect of mechanical milling induced strain and particle size reduction on some physical properties of polycrystalline yttrium iron garnet, Indian J. Phys. 89 (2015) 425–436, http://dx.doi.org/10.1007/s12648-014-0604-5.
[28] N. Chawake, R.S. Varanasi, B. Jaswanth, L. Pinto, S. Kashyap, N.T.B.N. Koundinya,

A.K. Srivastav, A. Jain, M. Sundararaman, R.S. Kottada, Evolution of morphology and texture during high energy ball milling of Ni and Ni-5wt% Cu powders, Mat. Charac. 120 (2016) 90–96, http://dx.doi.org/10.1016/j.matchar.2016.08.019.
[29] S. Oyarzún, A. Tamion, F. Tournus, V. Dupuis, M. Hillenkamp, Size effects in the magnetic anisotropy of embedded cobalt nanoparticles: from shape to surface, Sci. Rep. 5 (2015) 14749, http://dx.doi.org/10.1038/srep14749.
[30] M. Knobel, W.C. Nunes, L.M. Socolovsky, E. De Biasi, J.M. Vargas, J.C. Denardin, Superparamagnetism and other magnetic features in granular materials: a review on ideal and real systems, J. Nanosci. Nanotechnol. 8 (2008) 2836–2857, http://dx.doi.org/10.1166/jnn.2008.017.
[31] R.C. O'Handley, Modern Magnetic Materials: Principles and Applications Wiley, John Wiley & Sons, New York, 2000 ISBN 978-0-471-15566-9.
[32] V.K. Pecharsky, K.A. Gschneidner Jr., Magnetocaloric effect from indirect measurements: magnetization and heat capacity, J. Appl. Phys. 86 (1999) 565–575, http://dx.doi.org/10.1063/1.370767.
[33] D. Bloch, D.M. Edwards, M. Shimizu, J. Voiron, First order transitions in ACo_2 compounds, J. Phys. F. Met. Phys. 5 (1975) 1217, http://dx.doi.org/10.1088/0305-4608/5/6/022.
[34] J. Inoue, M. Shimizu, Volume dependence of the first-order transition temperature for RCo_2 compounds, J. Phys. F. Met. Phys. 12 (1982) 1811, http://dx.doi.org/10.1088/0305-4608/12/8/021.
[35] J. Inoue, M. Shimizu, First-and second-order magnetic phase transitions in $(RY)Co_2$ and R $(Co\text{-}Al)_2$ (R = heavy rare-earth element) compounds, J. Phys. F. Met. Phys. 18 (1988) 2487, http://dx.doi.org/10.1088/0305-4608/18/11/020.
[36] S. Khmelevskyi, P. Mohn, The order of the magnetic phase transitions in RCo_2 (R = rare earth intermetallic compounds, J. Phys. Condens. Matter 12 (2000) 9453, http://dx.doi.org/10.1088/0953-8984/12/45/308.
[37] M.A. Ruderman, C. Kittel, Indirect exchange coupling of nuclear magnetic moments by conduction electrons, Phys. Rev. 96 (1954) 99, http://dx.doi.org/10.1103/PhysRev.96.99.
[38] T. Kasuya, A theory of metallic ferro-and antiferromagnetism on Zener's model, Prog. Theor. Phys 16 (1956) 45–57, http://dx.doi.org/10.1143/PTP.16.45.
[39] K. Yosida, Magnetic properties of Cu-Mn alloys, Phys. Rev. 106 (1957) 893, http://dx.doi.org/10.1103/PhysRev.106.893.
[40] Q. Zhang, X.G. Liu, F. Yang, W.J. Feng, X.G. Zhao, D.J. Kang, Z.D. Zhang, Large reversible magnetocaloric effect in Dy_2In, J. Phys. D. Appl. Phys. 42 (2009) 055011, , http://dx.doi.org/10.1088/0022-3727/42/5/055011.
[41] R. Guetari, T. Bartoli, C.B. Cizmas, N. Mliki, L. Bessais, Structure, magnetic and magnetocaloric properties of new nanocrystalline $(Pr,Dy)Fe_9$ compounds, J. Alloys Compd. 684 (2016) 291–298, http://dx.doi.org/10.1016/j.jallcom.2016.05.170.
[42] A. Bezergheanu, E. Burzo, L. Chioncel, E. Dorolti, R. Tetean, Magnetic and electronic properties of nanocrystalline $Dy_xLa_{1-x}Ni_5$ compounds obtained by high energy ball milling, J. Optoeletronics Adv. Mater. 10 (2008) 805–808.
[43] N.K. Sun, F. Liu, Y.B. Gao, Z.Q. Cai, B.S. Du, S.N. Xu, P.Z. Si, Effect of microstrain on the magnetism and magnetocaloric properties of $MnAs_{0.97}P_{0.03}$, Appl. Phys. Lett. 100 (2012) 112407, , http://dx.doi.org/10.1063/1.3695039.
[44] T.B. Zhang, V. Provenzano, Y.G. Chen, R.D. Schull, Magnetic properties of a high energy ball-milled amorphous $Gd_5Si_{1.8}Ge_{1.8}Sn_{0.4}$ alloy, Sol. Stat. Comm. 147 (2008) 107, http://dx.doi.org/10.1016/j.ssc.2008.05.009.
[45] M. Venkat Narayana, S. Ganesh Kotnana, Jammalamadaka Narayana, Magnetocaloric effect and nature of magnetic transition in low dimensional $DyCu_2$, J. Alloys Compd. 683 (2016) 56–61, http://dx.doi.org/10.1016/j.jallcom.2016.05.042.
[46] S.D. Das, N. Mohapatra, K.K. Iyer, R.D. Bapat, E.V. Sampathkumaran, Magnetic behavior of nanocrystalline $ErCo_2$, J. Phys. Condens. Matter. 21 (2009) 296004, , http://dx.doi.org/10.1088/0953-8984/21/29/296004.
[47] P. Gorria, J.L. Sanchéz Llamazares, P. Álvarez, M.J. Pérez, J.S. Marcos, J.A. Blanco, Relative cooling power enhancement in magneto-caloric nanostructured Pr_2Fe_{17}, J. Phys. D. Appl. Phys. 41 (2008) 192003, , http://dx.doi.org/10.1088/0022-3727/41/19/192003.